

# The extracellular matrix protein agrin promotes heart regeneration in mice

Elad Bassat<sup>1</sup>, Yara Eid Mutlak<sup>2</sup>, Alex Genzelinakh<sup>1</sup>, Ilya Y. Shadrin<sup>3</sup>, Kfir Baruch Umansky<sup>1</sup>, Oren Yifa<sup>1</sup>, David Kain<sup>1</sup>, Dana Rajchman<sup>1</sup>, John Leach<sup>4</sup>, Daria Riabov Bassat<sup>5</sup>, Yael Udi<sup>5</sup>, Rachel Sarig<sup>1</sup>, Irit Sagi<sup>5</sup>, James F. Martin<sup>4</sup>, Nenad Bursac<sup>3</sup>, Shenhav Cohen<sup>2</sup> & Eldad Tzahor<sup>1</sup>

**The adult mammalian heart is non-regenerative owing to the post-mitotic nature of cardiomyocytes. The neonatal mouse heart can regenerate, but only during the first week of life. Here we show that changes in the composition of the extracellular matrix during this week can affect cardiomyocyte growth and differentiation in mice. We identify agrin, a component of neonatal extracellular matrix, as required for the full regenerative capacity of neonatal mouse hearts. *In vitro*, recombinant agrin promotes the division of cardiomyocytes that are derived from mouse and human induced pluripotent stem cells through a mechanism that involves the disassembly of the dystrophin-glycoprotein complex, and Yap- and ERK-mediated signalling. *In vivo*, a single administration of agrin promotes cardiac regeneration in adult mice after myocardial infarction, although the degree of cardiomyocyte proliferation observed in this model suggests that there are additional therapeutic mechanisms. Together, our results uncover a new inducer of mammalian heart regeneration and highlight fundamental roles of the extracellular matrix in cardiac repair.**

Heart disease, including myocardial infarction, is the leading cause of death worldwide. In mammals, post-mitotic adult cardiomyocytes have limited capacity to replenish damaged tissue<sup>1,2</sup>. Proliferation of cardiomyocytes and subsequent robust cardiac regeneration occur in lower vertebrates such as newt and zebrafish<sup>3</sup>. Notably, in neonatal mice, cardiomyocyte proliferation is sufficient to repair cardiac injuries; however, this ability is greatly diminished a week after birth<sup>4</sup>.

Heart pathologies involve extensive remodelling of the extracellular matrix (ECM) leading to formation of a rigid scar and reduced heart

function. The role of the ECM during cardiac regeneration remains largely unknown. Agrin is a large extracellular heparan sulfate proteoglycan that has been extensively studied because of its involvement in the formation of the neuromuscular junction. It triggers the aggregation of acetylcholine receptors via the muscle-specific kinase (MuSK)<sup>5,6</sup> and the low-density lipoprotein receptor-related protein 4 (Lrp4) receptor complex<sup>7</sup>. Agrin-mutant mice die around birth owing to disruption of

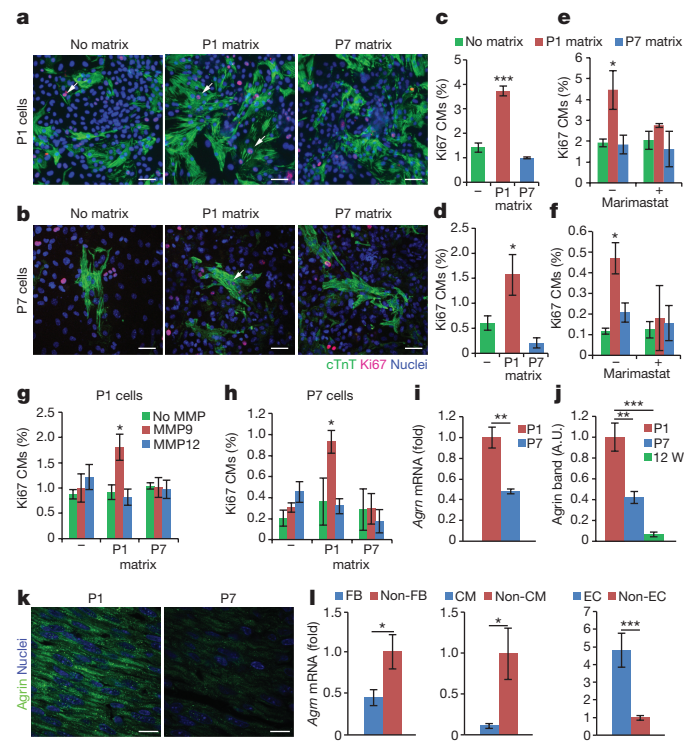


**Figure 1 | Identification of agrin in a screen for mouse cardiac ECM-mediated cardiomyocyte proliferation.** **a, b**, Representative fields of heart cultures stained with DAPI (blue), cTnT (green) and Ki67 (red). White arrows indicate Ki67<sup>+</sup>cTnT<sup>+</sup> cells. CMs, cardiomyocytes. **c, d**, Percentage of proliferating cardiomyocytes from P1 (**c**) or P7 (**d**) hearts in response to P1 and P7 ECM particles.  $n = 2,069$  cardiomyocytes from three samples (**c**);  $n = 2,221$  cardiomyocytes from four samples (**d**). **e, f**, Percentage of proliferating cardiomyocytes (Ki67<sup>+</sup>cTnT<sup>+</sup>) in response to P1 and P7 ECM in P1 (**e**) or P7 (**f**) cultures, with or without the broad MMP inhibitor (Marimastat).  $n = 3,480$  cardiomyocytes from three samples (**e**);  $n = 23,445$  cardiomyocytes from four samples (**f**). **g, h**, Percentage of P1 (**g**) or P7 (**h**) proliferating cardiomyocytes in response to MMP9- or MMP12-cleaved ECM fragments.  $n = 11,820$  cardiomyocytes from four samples (**g**);  $n = 15,509$  cardiomyocytes from four samples (**h**). **i**, qPCR of *Agrn* mRNA in P1 and P7 hearts. **j**, Quantification of western blots for agrin from P1, P7 and 12-week-old (12W) adult heart lysates. A.U., arbitrary units.  $n = 3$  samples per group. **k**, Images of P1 and P7 heart sections stained for agrin (green) and DAPI (blue).  $n = 3$  samples per group. **l**, qPCR analysis of cardiac populations (FB, fibroblasts; CM, cardiomyocytes; EC, endothelial cells).  $n = 4$  cardiomyocyte, 4 non-cardiomyocyte, 4 fibroblast, 4 non-fibroblast, 7 endothelial cells and 7 non-endothelial cell samples. Scale bars, 40  $\mu$ m (**a**) and 10  $\mu$ m (**k**). Data are presented as mean  $\pm$  s.e.m. \* $P < 0.05$ , \*\* $P < 0.01$ , \*\*\* $P < 0.001$ ; statistical significance was calculated using ANOVA followed by a Dunnett's post hoc test relative to the control group (**c–h**) or a Tukey's post hoc test (**j**), statistical significance was calculated using a one-tailed *t*-test (**i, l**).

<sup>1</sup>Department of Molecular Cell Biology, Weizmann Institute of Science, Rehovot 76100, Israel. <sup>2</sup>Faculty of Biology, Technion, Haifa 32000, Israel. <sup>3</sup>Department of Biomedical Engineering, Duke University, Durham, North Carolina 27708, USA. <sup>4</sup>Baylor College of Medicine and The Texas Heart Institute, Houston, Texas 77030, USA. <sup>5</sup>Department of Biological Regulation, Weizmann Institute of Science, Rehovot 76100, Israel.

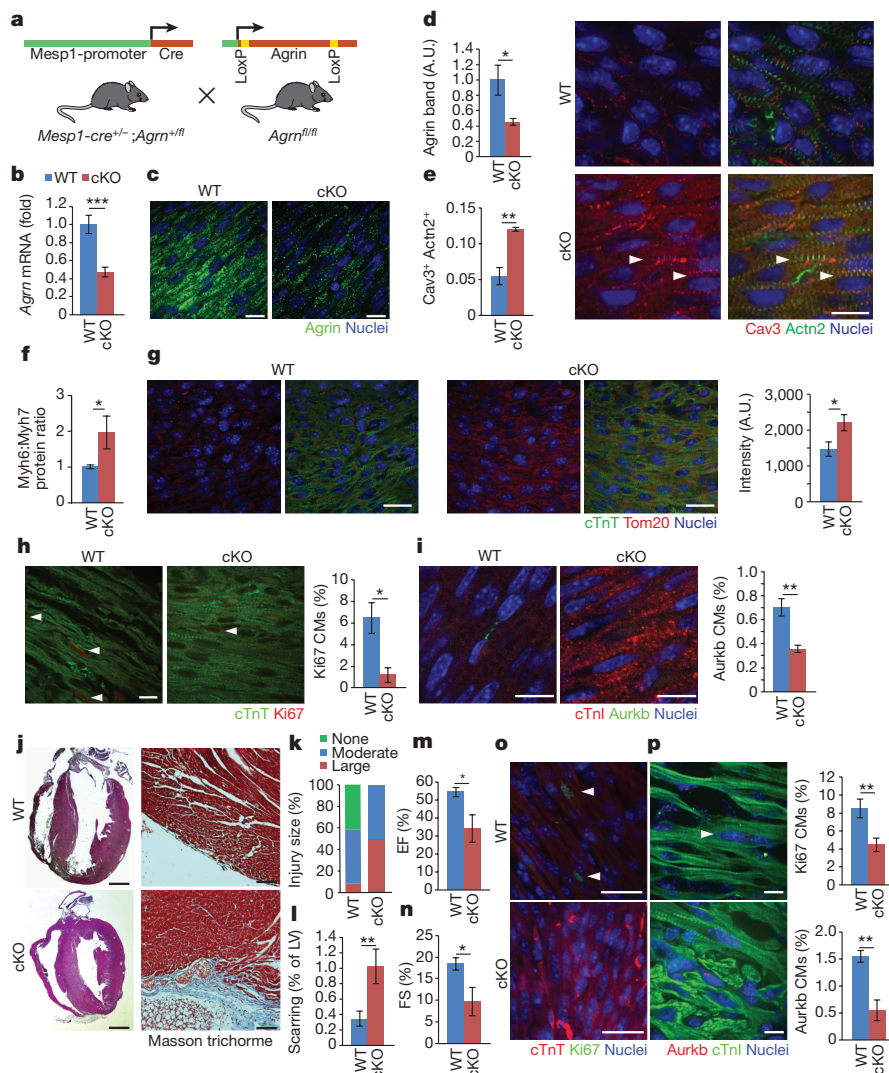


**Figure 2 | Agrin delays neonatal cardiomyocyte maturation and is required for P1 cardiac regeneration following surgical resection.** **a**, Diagram showing the mesoderm conditional knockout of agrin (agrin-cKO) in mice. **b**, qPCR of *Agrin* mRNA in P1 wild-type and agrin-cKO hearts. *n* = 8 wild-type (WT) and 7 cKO samples. **c**, Immunofluorescence images of agrin in P1 wild-type and agrin-cKO heart sections. *n* = 3 samples of each group. **d**, Quantification of western blots for agrin from wild-type and agrin-cKO mice heart lysates. *n* = 8 samples of each group. **e**, Immunofluorescence analysis and Pearson's correlation coefficient analysis of T-tubules labelled with Cav3 in the z-lines (as indicated by Actn2). *n* = 4 wild-type and 3 cKO samples. White arrow heads indicate colocalization of T-tubules and z-lines. **f**, Myh6:Myh7 protein ratio from wild-type and agrin-cKO mice. *n* = 5 wild-type and 6 agrin-cKO samples. **g**, Staining and mean pixel intensity quantification of mitochondrial content in cardiomyocytes measured by Tom20 staining. *n* = 5 wild-type and 3 agrin-cKO samples. **h, i**, *In vivo* evaluation of P1 cardiomyocyte cell-cycle markers (Ki67; **h**) and (Aurkb; **i**) by immunofluorescence analysis in wild-type and agrin-cKO left ventricle heart sections. *n* = 41,695 cardiomyocytes from 11 wild-type and 4 agrin-cKO samples

neuromuscular function.  $\alpha$ -Dystroglycan (Dag1) also serves as a receptor for agrin<sup>8</sup>. Membrane dystroglycan connects ECM components including agrin, laminin and perlecan to the cytoskeleton. Dag1 binds dystrophin and other associated proteins, known as the dystrophin-glycoprotein complex (DGC)<sup>9</sup>. Compromised integrity of the dystrophin protein and the DGC has been linked to numerous muscular dystrophies<sup>10</sup>. Mice lacking dystrophin (*Mdx*) show increased proliferation of cardiomyocytes at young ages<sup>11</sup>, yet upon myocardial infarction, display impaired cardiac regeneration and cytoskeletal remodelling<sup>12</sup>.

**(h)**; *n* = 3,212 cardiomyocytes from 3 samples per group (**i**). **j**, Histological sections of P1 resected wild-type and agrin-cKO mice, 28 days after injury, stained with Masson's trichrome. Bottom left corner of the cKO (left panel) was cropped to remove the adjacent section. **k, l**, Scar quantification of heart sections four weeks after resection of wild-type and agrin-cKO hearts. LV, left ventricle; none, 0% of the left ventricular wall; moderated  $\leq 1\%$  of the left ventricular wall; large  $\geq 1\%$  of the left ventricular wall. *n* = 12 wild-type and 8 cKO mice. **m, n**, Functional cardiac recovery measurements (ejection fraction (EF) and fractional shortening (FS)) of hearts from agrin-cKO and wild-type mice 28 days after resection. *n* = 5 wild-type and 3 cKO mice. **o, p**, *In vivo* evaluation of cardiomyocyte cell-cycle re-entry in the peri-infarct region by immunofluorescence analysis of Ki67 (**o**) or Aurkb (**p**) in heart sections 7 days after resection of wild-type and agrin-cKO hearts. *n* = 5,556 cardiomyocytes from seven wild-type and six cKO samples (**o**); *n* = 2,235 cardiomyocytes from three wild-type and four cKO samples (**p**). Scale bars, 10  $\mu$ m (**c, e, g-i, p**), 20  $\mu$ m (**o**), 100  $\mu$ m (**j**, right) and 1 mm (**j**, left). Data are presented as mean  $\pm$  s.e.m. \**P* < 0.05, \*\**P* < 0.01, \*\*\**P* < 0.001; statistical significance was calculated using a one-tailed *t*-test.

## Neonatal cardiac ECM induces cardiomyocyte proliferation

To study the role of the ECM in cardiac regeneration, we investigated the effect of cardiac ECM on cardiomyocyte turnover during the postnatal regenerative timeframe in mice<sup>4</sup>. Postnatal day (P)1 and P7 hearts were decellularized to produce cell-free ECM fragments (Extended Data Fig. 1a, b). *In vitro* administration of P1, but not P7, ECM fragments promoted an increase in cell-cycle activity in both P1 and P7 isolated cardiomyocytes (Fig. 1a-d). Co-treatment with a broad MMP

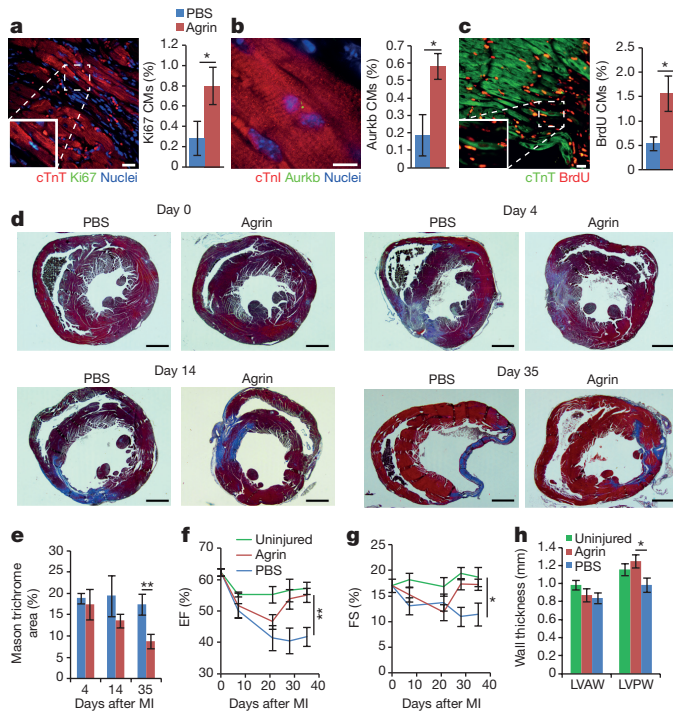


**Figure 3 | Agrin induces cardiac regeneration in adult mice.** **a–c**, *In vivo* evaluation of cardiomyocyte cell-cycle re-entry in the peri-infarct region seven days after myocardial infarction by Ki67 (**a**), Aurora kinase B (**b**) or 21 days after myocardial infarction BrdU (**c**).  $n = 1,842$  cardiomyocytes from five PBS and six agrin samples;  $n = 2,259$  cardiomyocytes from five samples per group (**b**);  $n = 9,307$  cardiomyocytes from six samples per group (**c**). For BrdU pulse-chase experiment see Methods. **d**, **e**, Heart section scar assessment following PBS or agrin treatment at indicated days after myocardial infarction (MI). Representative images are shown in **d** and quantified in **e**.  $n = 4$  mice per group for day 0, 5 PBS- and 4 agrin-treated mice for day 4, 4 PBS- and 5 agrin-treated mice for day 14, 7 PBS- and 8 agrin-treated mice for day 35. **f–h**, Serial echocardiographic measurements of ejection fraction, fractional shortening and wall thickness of uninjured and injured hearts treated with PBS or agrin. LVAW, left ventricle anterior wall; LVPW, left ventricle posterior wall.  $n = 8$  baseline, 5 uninjured, 6 PBS- and 8 agrin-treated mice (**f**, **g**);  $n = 2$  uninjured, 5 PBS- and 6 agrin-treated mice (**h**). Scale bars, 10  $\mu\text{m}$  (**a**, **c**), 20  $\mu\text{m}$  (**b**) and 1 mm (**d**). Data are presented as mean  $\pm$  s.e.m. \* $P < 0.05$ , \*\* $P < 0.01$ ; statistical significance was calculated using ANOVA followed by Dunnett's post hoc test relative to control group (**f–h**) or using a one-tailed *t*-test relative to PBS (**a–e**).

inhibitor (Marimastat) resulted in reduced cardiomyocyte proliferation induced by the P1 ECM (Fig. 1e, f). An *in situ* zymography assay measuring substrate cleavage specificity suggested the involvement of the gelatinase family of MMPs, MMP2 and/or MMP9 (Extended Data Fig. 1c–e). Indeed, MMP9-cleaved conditioned medium induced cardiomyocyte proliferation of P1 and P7 cells (Fig. 1g, h).

Liquid chromatography–mass spectrometry (LC–MS) analysis revealed that agrin was enriched in MMP9-cleaved P1 relative to P7 ECM fragments (Extended Data Fig. 2a). In addition, we identified Tgfb1, a parologue of periostin previously described as an inducer of cardiomyocyte proliferation<sup>13</sup>. We validated the expression levels of these genes by quantitative reverse transcription PCR (qRT–PCR) of P1 and P7 whole hearts (Extended Data Fig. 2b). Taken together, these results demonstrate the efficacy of this methodology for identifying ECM-associated molecules that promote cardiomyocyte proliferation *in vitro*.

### Agrin promotes cardiomyocyte proliferation *in vitro*

We next validated the downregulation of agrin expression between P1 and P7, as well as adult hearts by RNA, western blot and immunofluorescence analyses (Fig. 1i–k). P1 *Agrn* mRNA expression was

significantly enriched in the cardiac endothelial cell population relative to fibroblasts and cardiomyocytes (Fig. 1l and Extended Data Fig. 3).

We next tested whether recombinant rat agrin could induce cardiomyocyte proliferation in primary cardiac culture. Agrin dose-dependently increased P1 and P7 cardiomyocyte proliferation, as measured by immunofluorescence staining for cardiomyocytes markers (cardiac troponin T (cTnT) and Myh6) and markers of proliferation (Ki67, phospho-histone H3 (pH3) and aurora kinase B (Aurkb)), as well as by counting newly formed cardiomyocytes (Extended Data Fig. 4a–d). Together, these results indicate that agrin can stimulate cardiomyocyte proliferation *in vitro*.

### Agrin is required for cardiac regeneration in neonates

Because the reduction in agrin expression at P7 coincides with the loss of cardiac regenerative potential in mice, we determined its role during mouse neonatal cardiac regeneration. To avoid the perinatal lethality of *Agrn*-null mutants, we conditionally deleted *Agrn* in the cardiac mesoderm by crossing *MesP1*<sup>cre+/-</sup>; *Agrn*<sup>fl/fl</sup> mice with *Agrn*<sup>fl/fl</sup> mice (agrin-cKO) (Fig. 2a). Analysis of agrin protein and mRNA expression in agrin-cKO hearts confirmed that the allele was efficiently deleted (Fig. 2b–d). Agrin-cKO cardiomyocytes exhibited increased maturation of sarcomeric structures as determined by colocalization of sarcomeric  $\alpha$ -actinin and Cav3, a marker of transverse tubules (T-tubules)<sup>14</sup> (Fig. 2e). Likewise, quantification of the Myh6:Myh7 ratio by western blot (Fig. 2f) and staining of the mitochondrial marker Tom20 (Fig. 2g), was significantly increased in the agrin-cKO hearts. P1 agrin-cKO heart sections displayed increased striated sarcomere staining with reduced cardiomyocyte cell-cycle activity (Fig. 2h, i). Collectively, our results suggest that agrin suppresses cardiomyocyte maturation at neonatal stages (P1–P14; Fig. 2e–g and Extended Data Fig. 5a, b).

A mild increase in cardiomyocyte hypertrophy was evident in the agrin-cKO hearts (Extended Data Fig. 5c, d). Furthermore, agrin-cKO hearts exhibited a slight decrease in ejection fraction at one month, which disappeared at later time points (Extended Data Fig. 5e, f). Heart to body weight ratio and fibrotic staining were not affected (Extended Data Fig. 5g, h).

We also examined whether cardiac regeneration is impaired in agrin-cKO mice. P1 mice underwent cardiac resection and were assessed after one and four weeks (Extended Data Fig. 5i). Histological examination using Masson's trichrome staining showed increased fibrosis in the agrin-cKO mice relative to wild-type littermates (Fig. 2j–l), in line with reduced cardiac function (Fig. 2m, n and Extended Data Fig. 5j, k). Correspondingly, cardiomyocyte proliferation was reduced in agrin-cKO hearts (Fig. 2o, p). Taken together, these results demonstrate that agrin is necessary for cardiac regeneration in neonatal mice, but is not strictly required for cardiac growth or maintenance after birth.

### Agrin promotes regeneration after myocardial infarction

We next examined whether recombinant agrin could promote cardiomyocyte proliferation and cardiac regeneration at juvenile (Extended Data Fig. 6) and adult (Fig. 3) stages<sup>15</sup>. Mice were subjected to permanent ligation of the left anterior descending artery and treated with a single intramyocardial injection of agrin (50  $\mu\text{l}$  at 20  $\mu\text{g ml}^{-1}$ ) or PBS as control (Extended Data Fig. 6a). Agrin treatment induced moderate cardiomyocyte cell-cycle re-entry in the healthy myocardium adjacent to the infarcted region of both juvenile and adult hearts (Fig. 3a–c and Extended Data Fig. 6b, c). Histological analysis of adult hearts four days after myocardial infarction revealed that the damaged area was similar in both groups, however, from day 14 onwards, the scar area was reduced in the agrin-treated hearts, with a significant reduction by day 35 (Fig. 3d, e and Extended Data Fig. 6d). Furthermore, agrin treatment was sufficient to improve cardiac function following myocardial infarction, as evident by echocardiography in both models (Fig. 3f, g and Extended Data Fig. 6e, f). Agrin-treated mice also showed retention

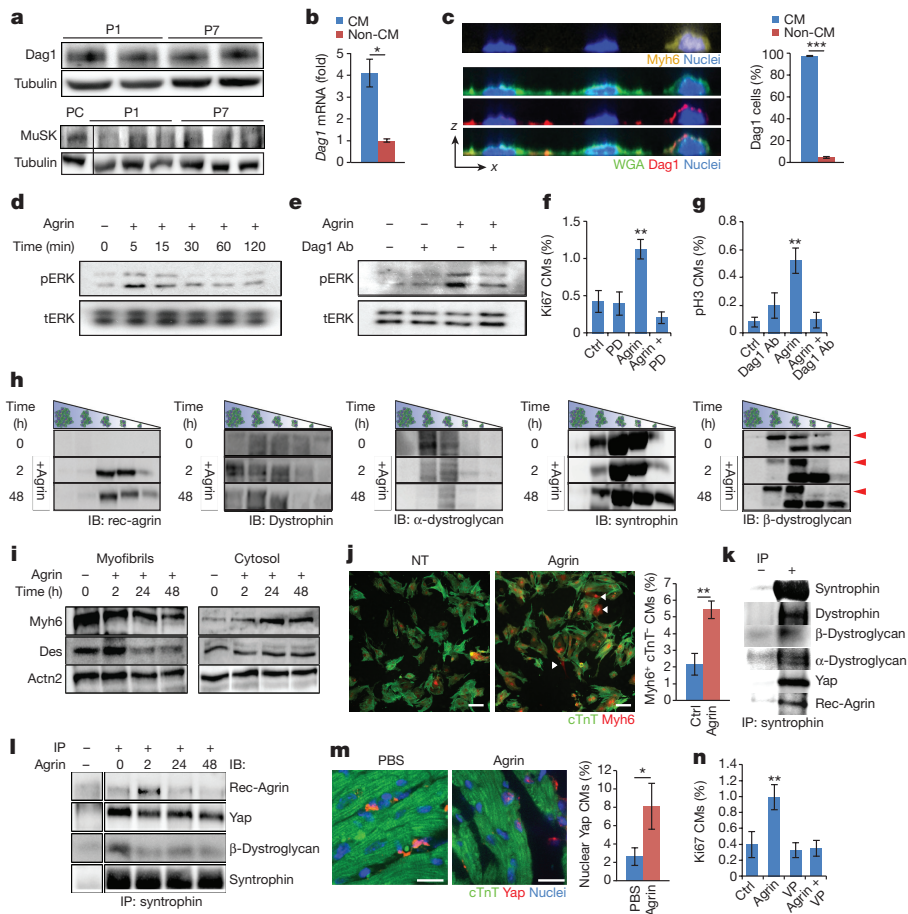


**Figure 4 | Agrin promotes cardiomyocyte proliferation through Dag1, ERK and Yap signalling.** **a**, Western blot of Dag1 and MuSK from P1 and P7 heart lysates.  $n = 3$  samples per group for MuSK,  $n = 6$  samples per group for Dag1. Skeletal muscle extract was used as positive control (PC) for MuSK expression (lower panel). **b, c**, P7 *Dag1* expression by qPCR (**b**) or membrane staining (**c**) in cardiomyocytes relative to non-cardiomyocytes ( $z$ - $x$  plane presented). WGA, wheat-germ agglutinin.  $n = 2$  cardiomyocyte and 2 non-cardiomyocyte RNA samples;  $n = 17,012$  cardiomyocytes from four samples per group (**c**). **d, e**, Western blots of phosphorylated ERK (pERK) and total ERK (tERK) in P7 cultures with the indicated treatments. Ab, antibody.  $n = 5$  samples (**d**);  $n = 3$  samples (**e**). **f, g**, P7 cardiomyocytes cell-cycle analysis by immunofluorescence staining following agrin treatment with a MEK inhibitor (**f**) or Dag1 inhibitory antibody (**g**). Ctrl, control; PD, PD0325901.  $n = 2,743$  cardiomyocytes from six samples (**f**);  $n = 6,649$  cardiomyocytes from four samples (**g**). **h**, Glycerol-gradient fractionation of whole-cell extracts from P7 cells with or without (time 0) agrin treatment for 2 and 48 h. Fractions were analysed by SDS-PAGE and immunoblotting (IB) with indicated antibodies.  $n = 3$  samples. Rec-agrin, recombinant agrin. Arrowheads indicate glycosylated form of  $\beta$ -dystroglycan. **i**, Isolated myofibrillar pellets and

cytosol from P7 cells treated with agrin for 48 h analysed by SDS-PAGE and immunoblotting.  $n = 3$  samples. **j**, Quantification of cardiomyocyte dedifferentiation using Myh6-lineage-derived cardiomyocytes (red mostly nuclear staining) stained with cTnT (green). Arrows indicate cardiomyocytes that have lost cTnT expression.  $n = 2,869$  cardiomyocytes from five samples per group. **k**, Co-immunoprecipitation (IP) assay of Yap, agrin and various DGC proteins immunoprecipitated with syntrophin.  $n = 3$  samples. **l**, Co-immunoprecipitation assay from 0, 2, 24 and 48 h agrin-treated cell membranes immunoprecipitated by syntrophin and blotted for Yap, agrin and other DGC proteins.  $n = 3$  samples. **m**, *In vivo* quantification of nuclear Yap of heart sections from 12-week-old mice with PBS or agrin treatments one day after myocardial infarction. Representative images are shown.  $n = 1,167$  cardiomyocytes from four mice per group. **n**, Cardiomyocyte proliferation assay of P7 heart cultures treated with agrin and the Yap-TEAD inhibitor. VP, verteporfin.  $n = 13,680$  cardiomyocytes from eight samples. Scale bars, 10  $\mu$ m (**j**) and 20  $\mu$ m (**m**). Data are presented as mean  $\pm$  s.e.m. \* $P < 0.05$ , \*\* $P < 0.01$ , \*\*\* $P < 0.001$ ; statistical significance was calculated using a one-tailed t-test (**b, c, j, m**) or ANOVA with Dunnett's post hoc test (**f, g, n**).

of wall thickness and protection from dilated cardiomyopathy, in contrast to control mice (Fig. 3h and Extended Data Fig. 6g).

The regenerative response to agrin begins 2 weeks after myocardial infarction peaking by 4–5 weeks. Such effect of a single dose of recombinant agrin prompted us to assess its pharmacokinetics. Agrin was detected in infarcted hearts up to 72 h after injection, although, as expected, its levels gradually decreased (Extended Data Fig. 7a, b).

### Agrin-Dag1 promotes DGC disassembly and Yap translocation

Previous reports on agrin signalling have highlighted Lrp4-MuSK,  $\alpha$ 3- $\text{Na}^+$ -ATPase and Dag1 as possible receptors mediating its activity<sup>7</sup>. *Dag1* was broadly expressed in P1 hearts (Extended Data Fig. 8a, b), but by P7 its RNA and protein expression were confined to

cardiomyocytes (Fig. 4a–c and Extended Data Fig. 3). By contrast, MuSK expression was very low in both P1 and P7 hearts (Fig. 4a), in agreement with published RNA-seqencing data<sup>16</sup>. In addition, we excluded the possibility that agrin acts through the  $\text{Na}^+$ - $\text{K}^+$  pump (Extended Data Fig. 8c).

During monocyte maturation, agrin-Dag1 signalling promotes ERK activation<sup>17</sup>. Similarly, we observed transient ERK activation following agrin treatment in P7 cardiac cell culture (Fig. 4d). Addition of a blocking antibody (IIH6C4) against the agrin-binding site of Dag1 diminished agrin-induced ERK activation (Fig. 4e). Furthermore, agrin-induced P7 cardiomyocyte proliferation was blocked using PD0325901 (MEK inhibitor) or the anti-Dag1 antibody (Fig. 4f, g).

To gain a deeper insight into agrin-mediated changes within the DGC, we treated P7 cardiac cultures with agrin for 2 and 48 h and

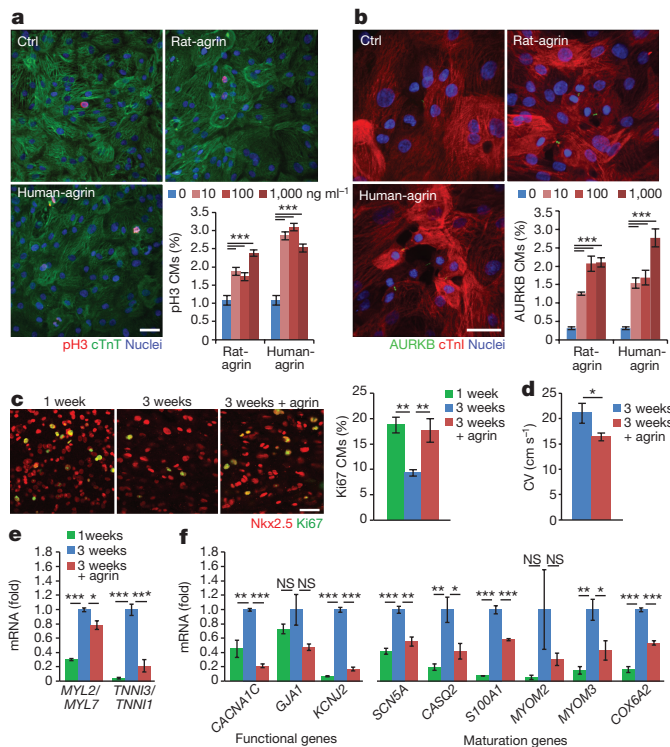


**Figure 5 | Agrin promotes proliferation and attenuates maturation of human iPSC-CMs.** **a, b**, Immunofluorescence of iPSC-CM cell-cycle activity by pH3 (**a**) or AURKB (**b**) in response to rat and human agrin administration (10–1,000 ng ml<sup>-1</sup>). Representative images of cultures treated with 1,000 ng ml<sup>-1</sup> are shown. pH3 quantification was performed automatically using imageXpress software ( $n = 174,850$  cardiomyocytes from 35 images of control (Ctrl) and 37 images of rat-agrin-treated cultures and 32 images for all other samples (**a**);  $n = 38,542$  cardiomyocytes from nine control samples and six samples in all other groups (**b**)). **c**, Human iPSC-CM proliferation assay in the 3D patch culture system.  $n = 3$  samples for one week, 4 samples for other treatments. Scale bars, 20  $\mu$ m (**a–c**). **d–f**, Effects of human agrin on conduction velocity (**d**) and structural and functional maturation genes (**e, f**).  $n = 4$  samples (**d**);  $n = 3$  samples per group (**e, f**). mRNA expression ratios of MYL2/MYL7 and TNNI3/TNNI1 are shown in **e**. CV, conduction velocity.  $n = 4$  samples (**d**);  $n = 3$  samples per group (**e, f**). Data are presented as mean  $\pm$  s.e.m. proliferation per field. \* $P < 0.05$ , \*\* $P < 0.01$ , \*\*\* $P < 0.001$ ; statistical significance was calculated using a one-tailed *t*-test (**d**) or relative to untreated or 3-week control group using ANOVA followed by Dunnett's post hoc test.

analysed whole-cell extracts by glycerol-gradient fractionation and SDS-PAGE (Fig. 4h). After 2 h of treatment, recombinant agrin was present in the same fractions containing DGC components, suggesting that agrin binds to this complex (Fig. 4h). Agrin treatment for 48 h resulted in reduced DGC integrity as evident by the shift of syntrophin, and the non-glycosylated form of  $\beta$ -dystroglycan to lighter glycerol-gradient fractions. Analysis of myofibrils isolated from cardiomyocytes treated with agrin revealed a gradual decrease in the myofibrillar content and accumulation in cytosolic fractions of Myh6,  $\alpha$ -actinin (Actn2) and Desmin (Des), indicating reduced integrity of the cytoskeleton and the myofibrillar apparatus, in line with a cardiomyocyte dedifferentiation process (Fig. 4i). We then asked whether agrin promotes cardiomyocyte dedifferentiation using *in vitro* assays for sarcomere integrity<sup>15,18</sup>. Agrin induced sarcomere disassembly in P7 cultured cardiomyocytes (Extended Data Fig. 8d) consistent with a 2.5-fold increase in the number of cardiomyocytes that completely lost cTnT expression following agrin treatment (Fig. 4j).

To investigate a possible link between agrin-DGC and the Hippo-signalling molecule Yap, we performed an experiment

using an anti-syntrophin antibody to immunoprecipitate DGC proteins, and blotted against members of the complex and Yap. Co-immunoprecipitation of the DGC components confirmed that both agrin and Yap were bound to the DGC (Fig. 4k). Following agrin treatment,  $\beta$ -dystroglycan and to a lesser extent, Yap, dissociated from the complex (Fig. 4l). Accordingly, the percentage of nuclear Yap in cardiomyocytes was increased 3–4-fold in adult hearts a day after myocardial infarction in response to agrin (Fig. 4m). Agrin failed to induce cardiomyocyte proliferation in the presence of verteporfin, an inhibitor of Yap-TEAD transcription activity (Fig. 4n). This result implicates a Yap-related signalling mechanism in cardiomyocyte proliferation induced by agrin. Together, our biochemical assays suggest that agrin binds to the DGC through Dag1 and reduces its stability, subsequently leading to myofibril disassembly and activation of downstream signalling molecules including Yap and ERK (Extended Data Fig. 9).

## Agrin affects proliferation and maturation of iPSC-CMs

To assess the translational potential of agrin, we examined whether agrin could promote proliferation of cardiomyocytes that are derived from human induced pluripotent stem cells (hiPSC-CMs) cultured on a gelatin-coated 2D substrate. Administration of either human or rat agrin dose-dependently increased hiPSC-CM cell-cycle activity (Fig. 5a, b). To explore whether agrin can also blunt the maturation process in hiPSC-CMs, we employed a 3D patch culture system and analysed the effects of human agrin on cardiomyocyte proliferation and structural and functional maturation<sup>19</sup>. Prolonged administration (100 ng ml<sup>-1</sup> for two weeks) of human agrin promoted a twofold increase in cardiomyocyte cell-cycle activity (Fig. 5c). Furthermore, agrin-treated cardiomyocytes in patches exhibited delayed maturation, as evident by reduced conduction velocity (Fig. 5d), and a significant reduction in the expression of a panel of functional and maturation markers (Fig. 5e, f). Taken together, in line with our findings in mice, human agrin promoted the proliferation and attenuated the maturation of human iPSC-CMs in both 2D and 3D culture systems.

## Discussion

We reveal previously unknown roles of agrin in the regulation of cardiomyocyte maturation around birth and we show that agrin can provide a stimulatory signal for cardiac regeneration upon injury in adult mice (Extended Data Fig. 9). Our study also raises new questions. We began the work searching for factors that would induce cardiomyocyte proliferation, but it is clear that agrin must have pleiotropic effects *in vivo*. Agrin-induced cardiomyocyte proliferation in adult mice is significantly lower compared to the genetic activation of ERBB2 signalling in cardiomyocytes<sup>15</sup>, suggesting that agrin treatment has other beneficial effects such as inhibition of fibrosis, modulation of the immune response and angiogenesis. Pharmacodynamic analysis suggested that following injection agrin is retained in the heart for three days, which is in line with a peak in cardiomyocyte proliferation seven days after treatment. The regenerative effect of agrin in adult mice occurs 3–5 weeks after injury, which was validated by two independent laboratories. This suggests that agrin exerts pleiotropic effects, in addition to mild cardiomyocyte proliferation that collectively intensify cardiac repair.

Agrin acts as a ligand for several receptors, including MuSK-Lrp4 and Dag1 (refs 9, 20). Given the inhibitory effect of anti-Dag1 antibody on the agrin-mediated response in cardiac cells, and the low levels of MuSK expression in the heart we conclude that agrin signals in cardiomyocytes via Dag1. We demonstrated that agrin binding to Dag1 promotes conformational changes that lead to a partial disassembly of the DGC, which serves as a mechanical bridge between the cardiac microenvironment and the inner contractile machinery (Extended Data Fig. 9). Therefore, in the neonatal heart, when endothelial-derived agrin levels are relatively high, it binds Dag1; in the adult, when agrin levels diminish, Dag1 can bind other ECM molecules, which are likely to contribute to cardiomyocyte cell-cycle arrest<sup>18</sup>.

Previous studies have demonstrated that atrophy of skeletal muscle is a step-wise process ultimately leading to the breakdown of myofibrils<sup>21,22</sup>. Biochemical analyses of DGC in cardiomyocytes treated with agrin showed the disassembly of the DGC. These findings provide biochemical insights and assays for cardiomyocyte dedifferentiation, showing temporal ligand-mediated sarcomere disassembly. In addition to its structural and mechanical characterization, recent studies suggest that the DGC acts as a signalling hub in skeletal muscle cells by tethering several signalling molecules<sup>23</sup>. DGC genes were recently shown to be targets of Yap, which has been intensively studied in the context of cardiac regeneration<sup>24–26</sup>.

We propose that cardiac regeneration includes mechanisms of DGC and/or myoskeleton destabilization (Extended Data Fig. 9). This model is in line with recent findings that link DGC/myoskeleton destabilization with enhanced ERBB2 signalling<sup>15,27</sup>, reduced Hippo signalling<sup>12</sup> and matrix rigidity<sup>18</sup>. Considering the multiple risks and technical problems associated with current cardiac regenerative strategies, agrin treatment shows potential as a relatively safe and effective agent for repairing damaged hearts.

**Online Content** Methods, along with any additional Extended Data display items and Source Data, are available in the online version of the paper; references unique to these sections appear only in the online paper.

Received 1 June 2016; accepted 12 May 2017.

Published online 5 June 2017.

1. Soopaa, M. H., Kim, K. K., Pajak, L., Franklin, M. & Field, L. J. Cardiomyocyte DNA synthesis and binucleation during murine development. *Am. J. Physiol. Heart Circ. Physiol.* **271**, H2183–H2189 (1996).
2. Bergmann, O. et al. Evidence for cardiomyocyte renewal in humans. *Science* **324**, 98–102 (2009).
3. Tzahor, E. & Poss, K. D. Cardiac regeneration strategies: staying young at heart. *Science* **356**, 1035–1039 (2017).
4. Porrello, E. R. et al. Transient regenerative potential of the neonatal mouse heart. *Science* **331**, 1078–1080 (2011).
5. Rupp, F., Payan, D. G., Magill-Solc, C., Cowan, D. M. & Scheller, R. H. Structure and expression of a rat agrin. *Neuron* **6**, 811–823 (1991).
6. Glass, D. J. et al. Agrin acts via a MuSK receptor complex. *Cell* **85**, 513–523 (1996).
7. Burden, S. J., Yumoto, N. & Zhang, W. The role of MuSK in synapse formation and neuromuscular disease. *Cold Spring Harb. Perspect. Biol.* **5**, a009167 (2013).
8. Bowe, M. A., Deyst, K. A., Leszyk, J. D. & Fallon, J. R. Identification and purification of an agrin receptor from Torpedo postsynaptic membranes: a heteromeric complex related to the dystroglycans. *Neuron* **12**, 1173–1180 (1994).
9. Henry, M. D. & Campbell, K. P. Dystroglycan: an extracellular matrix receptor linked to the cytoskeleton. *Curr. Opin. Cell Biol.* **8**, 625–631 (1996).
10. Campbell, K. P. & Kahl, S. D. Association of dystrophin and an integral membrane glycoprotein. *Nature* **338**, 259–262 (1989).
11. Richardson, G. D., Laval, S. & Owens, W. A. Cardiomyocyte regeneration in the *mdx* mouse model of nonischemic cardiomyopathy. *Stem Cells Dev.* **24**, 1672–1679 (2015).
12. Morikawa, Y. et al. Actin cytoskeletal remodeling with protrusion formation is essential for heart regeneration in Hippo-deficient mice. *Sci. Signal.* **8**, ra41 (2015).
13. Kuhn, B. et al. Periostin induces proliferation of differentiated cardiomyocytes and promotes cardiac repair. *Nat. Med.* **13**, 962–969 (2007).

14. Bian, W., Badie, N., Himmel, H. D., IV & Bursac, N. Robust T-tubulation and maturation of cardiomyocytes using tissue-engineered epicardial mimetics. *Biomaterials* **35**, 3819–3828 (2014).
15. D'Uva, G. et al. ERBB2 triggers mammalian heart regeneration by promoting cardiomyocyte dedifferentiation and proliferation. *Nat. Cell Biol.* **17**, 627–638 (2015).
16. O'Meara, C. C. et al. Transcriptional reversion of cardiac myocyte fate during mammalian cardiac regeneration. *Circ. Res.* **116**, 804–815 (2015).
17. Mazzon, C. et al. Agrin is required for survival and function of monocytic cells. *Blood* **119**, 5502–5511 (2012).
18. Yahalom-Ronen, Y., Rajchman, D., Sarig, R., Geiger, B. & Tzahor, E. Reduced matrix rigidity promotes neonatal cardiomyocyte dedifferentiation, proliferation and clonal expansion. *eLife* **4**, e07455 (2015).
19. Zhang, D. et al. Tissue-engineered cardiac patch for advanced functional maturation of human ESC-derived cardiomyocytes. *Biomaterials* **34**, 5813–5820 (2013).
20. Gesemann, M. et al. Alternative splicing of agrin alters its binding to heparin, dystroglycan, and the putative agrin receptor. *Neuron* **16**, 755–767 (1996).
21. Cohen, S., Zhai, B., Gygi, S. P. & Goldberg, A. L. Ubiquitylation by Trim32 causes coupled loss of desmin, Z-bands, and thin filaments in muscle atrophy. *J. Cell Biol.* **198**, 575–589 (2012).
22. Cohen, S., Nathan, J. A. & Goldberg, A. L. Muscle wasting in disease: molecular mechanisms and promising therapies. *Nat. Rev. Drug Discov.* **14**, 58–74 (2015).
23. Constantin, B. Dystrophin complex functions as a scaffold for signalling proteins. *Biochim. Biophys. Acta* **1838**, 635–642 (2013).
24. Heallen, T. et al. Hippo signaling impedes adult heart regeneration. *Development* **140**, 4683–4690 (2013).
25. Xin, M. et al. Hippo pathway effector Yap promotes cardiac regeneration. *Proc. Natl. Acad. Sci. USA* **110**, 13839–13844 (2013).
26. von Gise, A. et al. YAP1, the nuclear target of Hippo signaling, stimulates heart growth through cardiomyocyte proliferation but not hypertrophy. *Proc. Natl. Acad. Sci. USA* **109**, 2394–2399 (2012).
27. Reischauer, S., Arnaout, R., Ramadass, R. & Stainier, D. Y. R. Actin binding GFP allows 4D *in vivo* imaging of myofilament dynamics in the zebrafish heart and the identification of Erbb2 signaling as a remodeling factor of myofibril architecture. *Circ. Res.* **115**, 845–856 (2014).

**Supplementary Information** is available in the online version of the paper.

**Acknowledgements** This work was supported by grants to E.T. from the European Research Council, Israel Science Foundation and the Britain Israel Research and Academic Exchange (BIRAX). E.T., J.F.M. and N.B. are supported by Foundation LeDucq and NIH funding. We thank R. Burgess for providing the *Agrn<sup>f/f</sup>* mice. We thank Y. Levin, head of de Botton Institute for Protein Profiling, The Nancy and Stephen Grand Israel National Center for Personalized Medicine, for protein profiling. We thank E.T. and I.S. laboratory members, A. Navon, K. Yaniv and P. Riley for fruitful discussions, O. Goresh and B. Siani for animal husbandry, and N. Akron, D. Gorelik, R. Levine, S. Goldsmith, C. Raanan and M. Osin for genotyping and histology.

**Author Contributions** E.B., with help from A.G., performed most of the experiments. Y.E.M. and S.C. performed glycerol-gradient experiments. I.Y.S. and N.B. performed 3D iPSC-CM culture experiments. E.B., K.B.U., D.K., J.L. and J.F.M. performed *in vivo* animal experiments. O.Y. performed *in vitro* experiments. D.R.B. performed western blots. D.R. and R.S. performed hiPS-CM experiments. Y.U. and I.S. performed *in situ* zymography. E.T. supervised the project and with E.B. wrote the manuscript.

**Author Information** Reprints and permissions information is available at [www.nature.com/reprints](http://www.nature.com/reprints). The authors declare no competing financial interests. Readers are welcome to comment on the online version of the paper. Publisher's note: Springer Nature remains neutral with regard to jurisdictional claims in published maps and institutional affiliations. Correspondence and requests for materials should be addressed to E.T. (eldad.tzahor@weizmann.ac.il).

**Reviewer Information** *Nature* thanks K. Yutsey and the other anonymous reviewer(s) for their contribution to the peer review of this work.

## METHODS

**Isolation of cardiac cells.** Primary cardiac cells were isolated from P1 and P7 ICR mice using a neonatal dissociation kit (gentleMACS, Miltenyi Biotec) according to the manufacturer's instructions, and cultured in gelatin-coated wells (0.02%, G1393, Sigma-Aldrich) with DMEM/F12 medium supplemented with L-glutamine, Na-pyruvate, non-essential amino acids, penicillin, streptomycin, 5% horse serum and 10% fetal bovine serum (FBS) at 37 °C and 5% CO<sub>2</sub>. In experiments involving administration of either neural agrin (R&D Systems, dose range 10–1,000 ng ml<sup>-1</sup> *in vitro*), ECM fragments, MMP inhibitors (marimastat, Sigma-Aldrich), MEK inhibitor (PD0325901), 10 μM Yap inhibitor (verteporfin, Tocris)<sup>28,29</sup> or Dag1 inhibitory antibody (05-593, Millipore) the cells were allowed to adhere for 48 h before treatment. Subsequently, the medium was replaced with serum-free medium containing the indicated treatments for 72 h. Cells were fixed in 4% paraformaldehyde (PFA) and stained for markers of interest.

**Extraction of heart-derived ECM.** Hearts were collected from P1 and P7 ICR mice and washed with phosphate-buffered saline (PBS), embedded in OCT and frozen at –20 °C. Hearts were cut transversely into 100-μm fragments using a cryostat and immersed in 2% Triton X-100 and 20 mM EDTA solution in DDW overnight at room temperature. The remaining matrices were washed with PBS and subsequently placed in 10% penicillin-streptomycin-amphotericin B solution (Biological Industries) for sterilization. Prior to matrix administration to culture, fragments were washed with serum-free medium (as previously described) and homogenized using gentleMACS M tubes (Miltenyi Biotec). In experiments containing ECM cleaved peptides, ECM fragments were treated with MMPs for 24 h at 30 °C than filtered to remove residual debris before incubation with the cells.

**Scanning electron microscopy.** Samples were fixed in a solution of 0.1 M cacodylate buffer (pH 7.4) containing 2.5% PFA and 2.5% glutaraldehyde pH 7.2, for 30 min at room temperature and washed three times in the same buffer. The cells were postfixed in 1% osmium tetroxide in the cacodylate buffer for 30 h and washed with three changes of the buffer. The samples were then stained with 4% sodium silicotungstate (pH 7) for 45 min and dehydrated through an ethanol series increasing in concentration to 100% ethanol. After that the samples were dried in a critical point dryer and placed on a stub followed by pressure from placing another stub on top of them. The sample fractures were coated with gold-sputter for imaging with an Ultra 55 Feg Zeiss SEM operating at 2 kV.

**Tissue-culture immunostaining.** Adherent cells were grown on a gelatin-coated 96-well plate. The cells were fixed with 4% PFA in PBS for 10 min and permeabilized with 0.2% Triton X-100 in PBS for 5 min, and blocked with PBS containing 0.1% Triton and 3% bovine serum albumin (BSA) for 1 h at room temperature. For immunostaining, the cells were incubated for 2 h with the following monoclonal antibodies diluted in the blocking solution: anti-cTnT (1:200, ab33589, Abcam), anti-cTnI (1:200, ab47003, Abcam), anti-Nkx2.5 (1:300, sc-8697, Santa Cruz), anti-Dag1 (1:200, sc-28534, Santa Cruz) antibodies were used to identify cardiomyocytes; anti-Ki67 antibody (1:200, 275R, Cell Marque), anti-phosphorylated histone 3 (pH3) (1:200, SC-8656-R, Santa Cruz Biotechnology) and anti-aurora kinase B (AURKB, 1:100, 611082, BD Transduction Laboratories) antibodies were used to analyse cell-cycle re-entry, DNA synthesis, karyokinesis and cytokinesis, respectively. Cells were then washed three times with PBS and stained for 45 min at room temperature with suitable secondary antibody. This was followed by 5 min of DAPI (4,6-diamidino-2-phenylindole dihydrochloride). The cells were viewed under Nikon fluorescence or an Olympus live-cell imaging microscope.

**Proteomic analysis.** For analysis of P1 and P7 ECM products released by MMP9 (as described above), samples were subjected to in-solution digestion and ion-intensity-based label-free quantification. Quantitation of the peptides revealing specific cleavage substrates was conducted using the Scaffold software (Proteome Software Inc.). Bioinformatic analysis was performed to distinguish between ECM and non-ECM molecules.

**Separation of distinct cardiac cell populations.** Primary cardiac cells were isolated from P1 and P7 mice using a neonatal dissociation kit (gentleMACS) according to the manufacturer's instructions. Separation to distinct cardiac cell populations was performed by using the Neonatal Cardiac Endothelial Cell Isolation kit (130-104-183, Miltenyi Biotec), Neonatal Cardiac Fibroblast Cell Isolation kit (130-101-372, Miltenyi Biotec) or by Neonatal Cardiomyocyte Isolation kit (130-100-825, Miltenyi Biotec), according to the manufacturer's instructions.

**Quantitative real-time PCR (qRT-PCR).** Total RNA was isolated using the nucleospin RNA II kit (Macherey Nagel) according to the manufacturer's protocol. cDNA was synthesized by using the High Capacity cDNA Reverse Transcription Kit (Applied Biosystems) according to the manufacturer's protocol. qRT-PCR was performed using SYBRGreen PCR Master Mix (Applied Biosystems) on a StepOnePlus Real-Time PCR system (Applied Biosystems). Values for specific genes were normalized to *Hprt* housekeeping control.

**Western blot analysis.** Western blotting was performed with the SDS-PAGE Electrophoresis System. Total heart tissue extracts were prepared and transferred to PVDF membranes. The following primary antibodies were used: anti-Agrn (ab85174, Abcam), anti-α-dystroglycan (05-298, Millipore), anti-Gapdh (2118, Cell signaling technologies), anti-MuSK (WH0004593M1, Sigma-Aldrich), anti-Myh6 (ab50967, Abcam), anti-Myh7b (ab172967, Abcam), anti-cTnT (ab33589, Abcam) and anti-cTnI (ab47003, Abcam), anti-ERK2 (sc-154, Santa Cruz), anti-phospho-ERK (4370, Cell Signaling), and anti-α-tubulin (T5168, Sigma-Aldrich). Horseradish peroxidase anti-mouse, anti-rabbit or anti-goat (Sigma-Aldrich) was used as secondary antibody.

**Immunofluorescence analysis.** Heart sections underwent deparaffinization and microwave antigen retrieval in EDTA or citric acid buffer, followed by gradual chilling. Samples were permeabilized with 0.5% Triton X-100 in PBS for 5 min and blocked with 5% BSA in PBS containing 0.1% Triton for 1 h at room temperature. Then, samples were incubated overnight at 4 °C with the following antibodies diluted in 3% BSA blocking solution and 1% horse serum: anti-cTnT (1:200, ab33589, Abcam), anti-cTnI (1:200, ab47003, Abcam) and anti-α-actinin (1:200, A7811, Sigma-Aldrich) antibodies were used to identify cardiomyocytes; anti-Ki67 antibody (1:200, 275R, Cell Marque), anti-pH3 (1:200, SC-8656-R, Santa Cruz Biotechnology) and anti-aurora kinase B (AURKB, 1:100, 611082, BD Transduction Laboratories) antibodies were used to analyse cell-cycle re-entry, DNA synthesis, karyokinesis and cytokinesis, respectively. Other antibodies used in the study included anti-Agrn (1:200, sc-374117, Santa Cruz), anti-Cav3 (1:200, ab2912, Abcam), anti-Tom20 (1:200, sc-11415, Santa Cruz) and anti-Yap (1:200, NB110-58358, Novus). After three 10-min washes with PBS, samples were stained for 1 h at room temperature with fluorescent secondary antibodies (Abcam) followed by 10 min of DAPI staining for nucleus visualization. Slides were mounted with Immuno-mount (9990412, Thermo Scientific) and viewed under a fluorescence microscope (Nikon Intensilight Nikon Eclipse 90i, Nikon or Olympus live-cell imaging microscope) or spinning-disc confocal microscope (Carl Zeiss). Colocalization Pearson's correlation coefficient analysis was performed using the Imaris software. In all cell counting experiments fields of view were randomized to reduce counting bias.

**Live counting of cardiomyocyte number.** *Myh6-cre;ROSA26-tdTomato* cardiac cells were isolated and automatically plated on optical-bottom plastic 96-well plates pre-coated with 0.02% gelatin, using a Multi Drop machine, and treated with either agrin or other known Na<sup>+</sup>K<sup>+</sup> channel inhibitors from compound libraries, as previously described. Cardiomyocyte detection was performed using the TTP Labtech's acumen system and Cellista software. Cardiomyocyte number change was assessed using Accelrys Pipeline Pilot software, relative to initial cardiomyocyte numbers in each individual well.

**Mouse experiments.** All experiments were approved by the Animal Care and Use Committee of the Weizmann Institute of Science. All myocardial infarction experiments were performed on ICR mice. Surgeries on adult mice were performed only on 12-week-old females, while no such gender selection took place for surgeries on P7 juvenile mice.

To track the cardiac muscle cell lineage, we intercrossed *Myh6-cre* mice with *ROSA26-tdTomato* mice. *Myh6-cre* mice carry the *cre*-coding sequence inserted after the α-myosin heavy chain promoter (*Myh6*), which can drive high-efficiency gene recombination in cardiomyocytes. *ROSA26-tdTomato* indicator mice have a conditional red fluorescent protein (RFP) variant allele that requires Cre-mediated recombination for expression. This system allowed us to clearly visualize RFP-labelled cardiomyocytes in culture. *ROSA26-tdTomato* and *Myh6-cre* mice were maintained on a C57BL/6 background. To test the effect of agrin in cardiac regeneration, we intercrossed *Agrn<sup>f/f</sup>* to *Agrn<sup>f/f</sup>;Mesp1-cre* mice. The *Mesp1* promoter is expressed in the mesodermal cell lineage during early gastrulation and marks the most primitive multipotent cardiac progenitors, which affects the majority of heart cells (cardiomyocytes, fibroblasts and endothelial cells). *Agrn<sup>f/f</sup>;Mesp1-cre* mice were maintained on a C57BL/6 background.

**Apical resection.** Apical resection of P1 mice was performed by surgical removal of the outmost apical region of the heart. P1 mice were anaesthetized by cooling on an ice bed for 3 min. Following skin incision, lateral thoracotomy at the third intercostal space was performed by blunt dissection of the intercostal muscles. Following resection thoracic wall incisions were sutured with 5.0 non-absorbable silk sutures, and the wound was closed using skin adhesive. Mice were then warmed for several minutes until recovery.

**Myocardial infarction.** Myocardial infarction at juvenile (P7) or adult stage was induced by ligation of the left anterior descending (LAD) coronary artery. P7 mice were anaesthetized by cooling on an ice bed for 4 min, whereas adult mice were sedated with isoflurane (Abbott Laboratories) and, following tracheal intubation, were artificially ventilated. Following skin incision, lateral thoracotomy at the third intercostal space was performed by blunt dissection of the intercostal muscles.

Following artery ligation, intramyocardial injections of agrin ( $50\text{ }\mu\text{l}$  at  $1\text{ }\mu\text{g}$  per mouse) or PBS were administered. Then, thoracic wall incisions were sutured with 6.0 non-absorbable silk sutures, and the wound was closed using skin adhesive. Mice were then warmed for several minutes until recovery. To record cell proliferation *in vivo*,  $50\text{ mg kg}^{-1}$  BrdU was injected intraperitoneally daily, for 10 days following myocardial infarction. Hearts were collected after 21 days and subjected to BrdU immunohistochemistry using an anti-BrdU antibody (Ab) (MCA2060, Serotec).

**Echocardiography.** Heart function was evaluated by transthoracic echocardiography performed on isoflurane-sedated mice using a Vevo 770 VisualSonics device for juvenile and short axis measurements of adult mice and Vevo 3100 for neonatal and adult mice. All echocardiography measurements were performed in a blinded manner.

**Histology.** Mouse heart tissues were fixed in 4% PFA and sectioned. For analysis of juvenile and adult cardiac regeneration following myocardial infarction, paraffin sections were cut through the entire ventricle from apex to base into serial sections at 0.4 mm intervals. For analysis of neonatal cardiac regeneration following resection, paraffin sections were cut frontally to include base-to-apex in each section. Haematoxylin and eosin (H&E) staining and Masson's trichrome staining were performed according to standard procedures and used for detection of fibrosis. Scar size was quantified in the section containing the papillary muscle region using ImageJ software, based on Masson's trichrome staining. Adult and juvenile scar size was calculated relative to total section size, whereas neonatal scar size was calculated relative to left ventricle size.

**Immunoprecipitation.** For protein extract preparation, PBS- or agrin-treated hearts were flash-frozen in liquid nitrogen, and homogenized in RIPA buffer. To immunoprecipitate His-tagged recombinant agrin, 5 mg of total extract were subjected to immunoprecipitation using Ni-NTA resin (88221, Thermo Scientific), according to the manufacturer's protocol, with minor changes: immunoprecipitation duration was overnight, and elution was performed using 0.5 M imidazole, and not as stated.

**Homogenization of cardiomyocytes.** For preparation of whole-cell extracts, cardiomyocytes were lysed in homogenization buffer (20 mM Tris-HCl pH 7.2, 5 mM EGTA, 100 mM KCl, 1% Triton X-100, PMSF, Phosphostop and protease inhibitors mix) and centrifuged at 6,000g for 20 min at  $4^\circ\text{C}$  to pellet nuclei, myofibrils and unbroken cells.

In cell-fractionation experiments, cardiomyocytes were homogenized in buffer C (20 mM Tris-HCl pH 7.6, 100 mM KCl, 5 mM EDTA, 1 mM DTT, 1 mM sodium orthovanadate, 1 mM PMSF, Phosphostop and protease inhibitors mix) and centrifuged at 2,900g for 20 min at  $4^\circ\text{C}$ . The obtained supernatant (containing cytosol and plasma membranes) and myofibrillar pellet (containing myofibrils and nuclei) were processed separately as follows. The supernatant was centrifuged at 180,000g for 90 min using a TLA-55 rotor (Beckman Coulter). The acquired pellet was re-suspended in buffer M (20 mM Tris-HCl pH 7.6, 100 mM KCl, 5 mM EDTA, 1 mM DTT, 0.25% sodium deoxycholate, 1% NP-40, 1 mM sodium orthovanadate,  $10\text{ }\mu\text{g ml}^{-1}$  leupeptin, 3 mM benzamidine and 1 mM PMSF), incubated at  $4^\circ\text{C}$  for 20 min, and after a final centrifugation (30 min at 100,000g and  $4^\circ\text{C}$ ) the supernatant was collected as purified plasma membrane fraction. To obtain a nuclear fraction, the myofibrillar pellet was washed twice in buffer C, resuspended in buffer N (20 mM HEPES pH 7.9, 1.5 mM MgCl<sub>2</sub>, 500 mM NaCl, 5 mM EDTA, 20% glycerol, 1% Triton X-100, 1 mM sodium orthovanadate,  $10\text{ }\mu\text{g ml}^{-1}$  leupeptin, 3 mM benzamidine, 1 mM PMSF and 50 mM NaF), and following incubation on ice for 30 min and a final centrifugation (9,000g for 30 min at  $4^\circ\text{C}$ ), the supernatant was collected as isolated nuclear fraction.

**Glycerol-gradient fractionation.** To isolate the DGC and associated proteins,  $100\text{ }\mu\text{g}$  of whole cardiomyocytes extract was loaded on a 10–40% glycerol gradient and centrifuged for 24 h at 35,000 r.p.m. using a MLS-50 Swinging-Bucket rotor (Beckman Coulter). Fractions collected from glycerol gradients were subjected to trichloroacetic acid (TCA) precipitation (10%) and precipitates were analysed by SDS-PAGE and immunoblotting. The following primary antibodies were used: anti-rat recombinant Agrn (MAB550, R&D systems), anti- $\alpha$ -dystroglycan (sc-28534, Santa Cruz), anti- $\beta$ -dystroglycan (Mandag2[7d11], DSHB), anti-syntrophin (sc-50460, Santa Cruz), anti-dystrophin (ab15277, Abcam), anti-Grb2

(sc-8034, Santa Cruz), anti-Myh6 (ab50967, Abcam), anti-actin (A2066, Sigma-Aldrich), anti-Actn1 (A2543, Sigma-Aldrich), anti-Des (ab8592, Abcam), anti-Yap (sc-15407, Santa Cruz) and anti-H3f3a (ab62642, Abcam). Horseradish peroxidase anti-mouse, anti-rabbit or anti-goat (Sigma-Aldrich) was used as secondary antibody.

**Immunoprecipitation of  $\alpha$ -1-syntrophin.** To determine whether agrin binds DGC and Yap, the DGC component  $\alpha$ -1-syntrophin was immunoprecipitated from whole-cell extracts (180  $\mu\text{g}$ ) of cardiomyocytes treated with recombinant agrin for 2 h. Following an overnight incubation on a rotating device at  $4^\circ\text{C}$ , protein A/G agarose was added for additional 4 h, and precipitates were subsequently washed with buffer W (20 mM Tris-HCl pH 7.6, 150 mM NaCl, 1 mM EGTA, 1 mM EDTA, 0.1% Triton, 2.5 mM sodium pyrophosphate,  $1\text{ }\mu\text{g ml}^{-1}$  leupeptin and 1 mM PMSF) and were analysed by immunoblotting using specific antibodies.

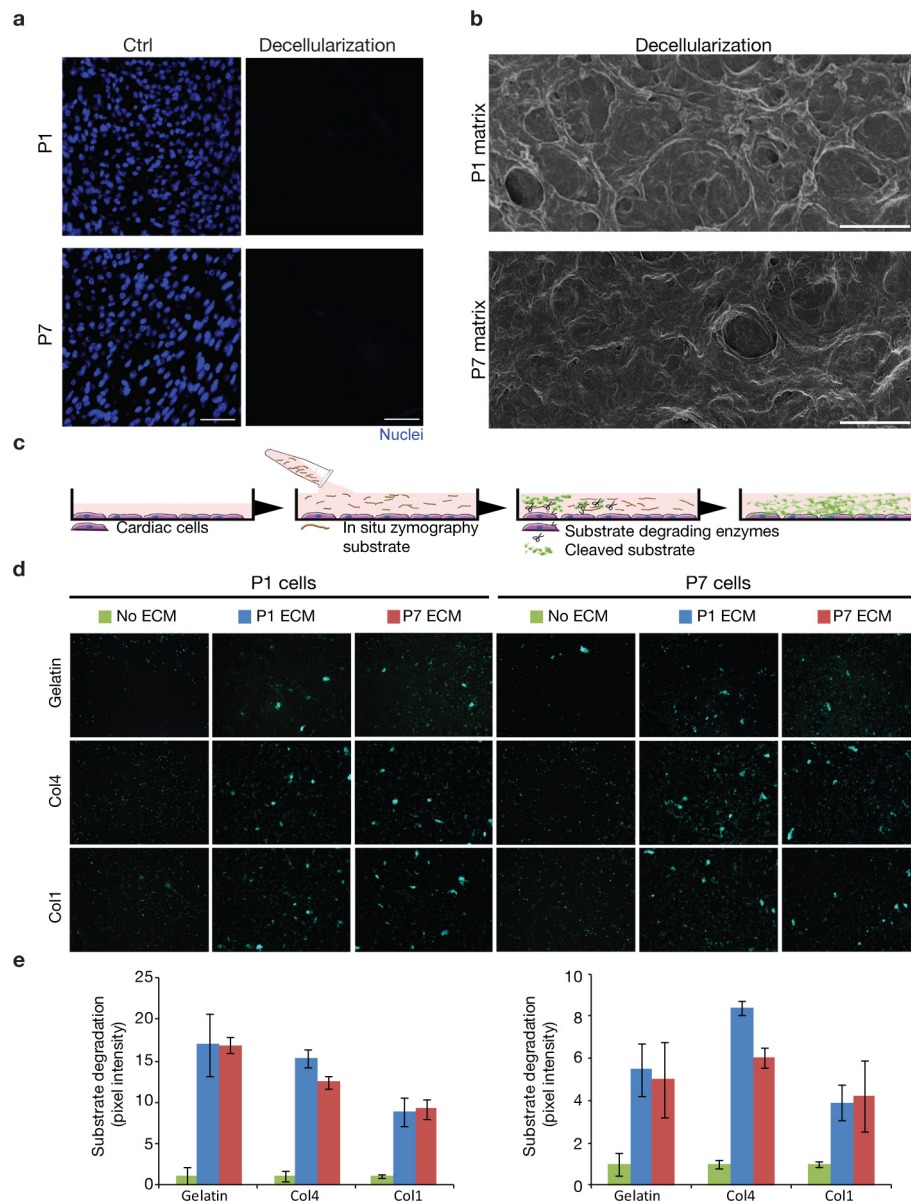
**Human iPSC-CM cultures.** Cardiomyocytes derived from iPSCs (Cellular Dynamics International (CDI)) were thawed and  $1 \times 10^5$  cells were seeded on 0.02% gelatin-coated 96-well optical bottom plates according to the manufacturer's instructions. The cells were allowed to adhere for 48 h before maintenance medium exchange and fresh medium was replaced every other day. After one week, the cells were treated with human perlecan, human agrin or rat agrin (concentrations ranging between 10 and 1,000 ng ml<sup>-1</sup>), which were replenished every other day. The cells were treated for four days before fixation and staining (as previously described).

**Agrin treatment in 3D hiPSC-CM cardiac tissues.** Wild-type DU11 hiPSC cells (derived and validated at Duke University) were maintained as feeder-free cultures on growth-factor-reduced Matrigel (Corning) in E8 medium (Stem Cell Technologies) and passaged as small clusters (10–20 cells) with EDTA every 4–5 days. hiPSC cells were dissociated as single cells with Accutase and differentiated into cardiomyocytes via small molecule (CHIR99021 and IWP-4) based modulation of Wnt signalling. hiPSC-CMs were purified using glucose-free, lactate-based metabolic selection on day 10–12 of differentiation, replated on day 12 to remove apoptotic cells and debris, and dissociated for incorporation into 3D tissues on day 21 using previously established methods. In brief,  $0.5 \times 10^6$  cells were combined with a hydrogel solution (2 mg ml<sup>-1</sup> fibrinogen, 10% Matrigel, 1 U ml<sup>-1</sup> thrombin) and polymerized around a  $9 \times 9$  mm Cerex frame inside polydimethylsiloxane (PDMS, Dow Corning) square moulds. Cardiac patches were removed from moulds and cultured on a rocking platform (GeneMate Rocker, BioExpress) for three weeks. Cardiac media was switched from 3D RB+ (RMPI 1640, 2% B27) to 5% FBS media (low-glucose DMEM, 5% FBS) at one week of culture, as previously described<sup>30</sup>.

For agrin treatment, hiPSC-CM patches were treated with agrin (100 ng ml<sup>-1</sup>) from day 7–21 of 3D culture. Optical mapping of action potentials was performed after 1–3 weeks of culture per established methods. hiPSC-CM cardiac patches were incubated with di-4-ANEPPS (15  $\mu\text{M}$ , Life Technologies) in standard Tyrodes' solution containing 5  $\mu\text{M}$  blebbistatin (to inhibit contractions and eliminate motion artefacts) and stimulated from a corner with a bipolar platinum electrode (8–15 V). Propagation of electrical impulses was recorded on a 504-channel photodiode array (RedShirt Imaging), and conduction velocity was calculated using custom MATLAB algorithms. Total RNA was isolated at 1 and 3 weeks of culture (Bio-Rad kit). cDNA was synthesized using an iScript cDNA synthesis kit (Bio-Rad), and qPCR reactions were run in duplicates using iTaq SYBR green Supermix (Bio-Rad) and human-specific primers (Supplementary Table 2) on an ABI 7900HT Fast Real-Time PCR system (Applied Biosystems). Relative expression was quantified using the  $\Delta\Delta\text{C}_t$  method with GAPDH as the housekeeping gene.

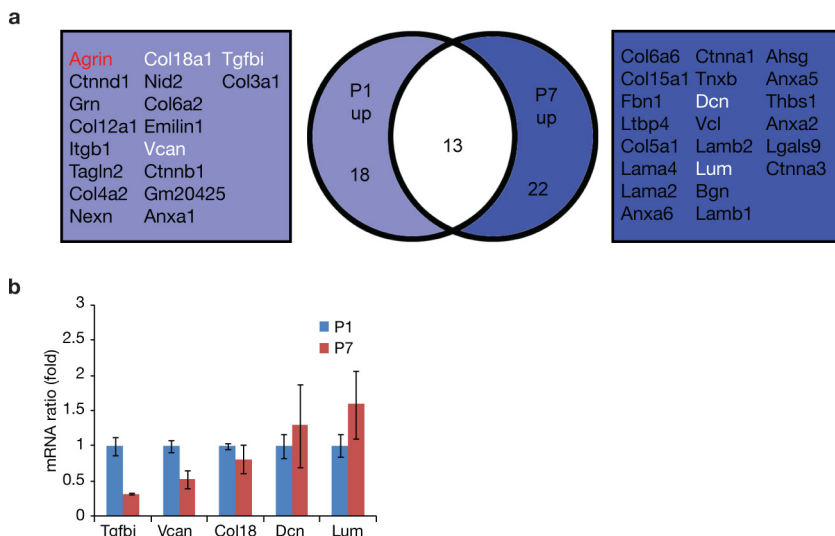
**Data availability.** Source Data are provided in the online version of the paper or are available from the corresponding author upon request.

28. Liu-Chittenden, Y. et al. Genetic and pharmacological disruption of the TEAD-YAP complex suppresses the oncogenic activity of YAP. *Genes Dev.* **26**, 1300–1305 (2012).
29. Wang, C. et al. Verteporfin inhibits YAP function through up-regulating 14-3-3 $\sigma$  sequestering YAP in the cytoplasm. *Am. J. Cancer Res.* **6**, 27–37 (2015).
30. Jackman, C. P., Carlson, A. L. & Bursac, N. Dynamic culture yields engineered myocardium with near-adult functional output. *Biomaterials* **111**, 66–79 (2016).

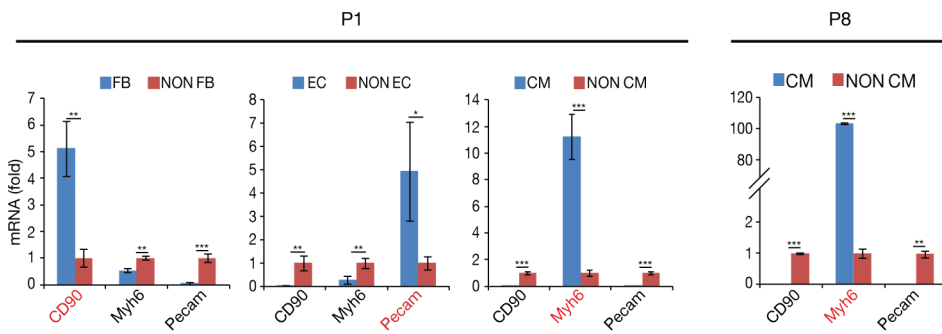


**Extended Data Figure 1 | P1 and P7 ECM explants contain increased gelatinase activity. **a, b**, Cell removal assessment of heart sections by DAPI or scanning electron microscopy. Scale bars, 50 µm (**a**) and 20 µm (**b**). **c**, A schematic diagram of the *in situ* zymography assay.**

**d**, Immunofluorescence evaluation of Col1, Col4 and gelatin degradation in response to P1 and P7 ECM. **e**, Quantification of the *in situ* zymography assay.  $n = 2$  samples.

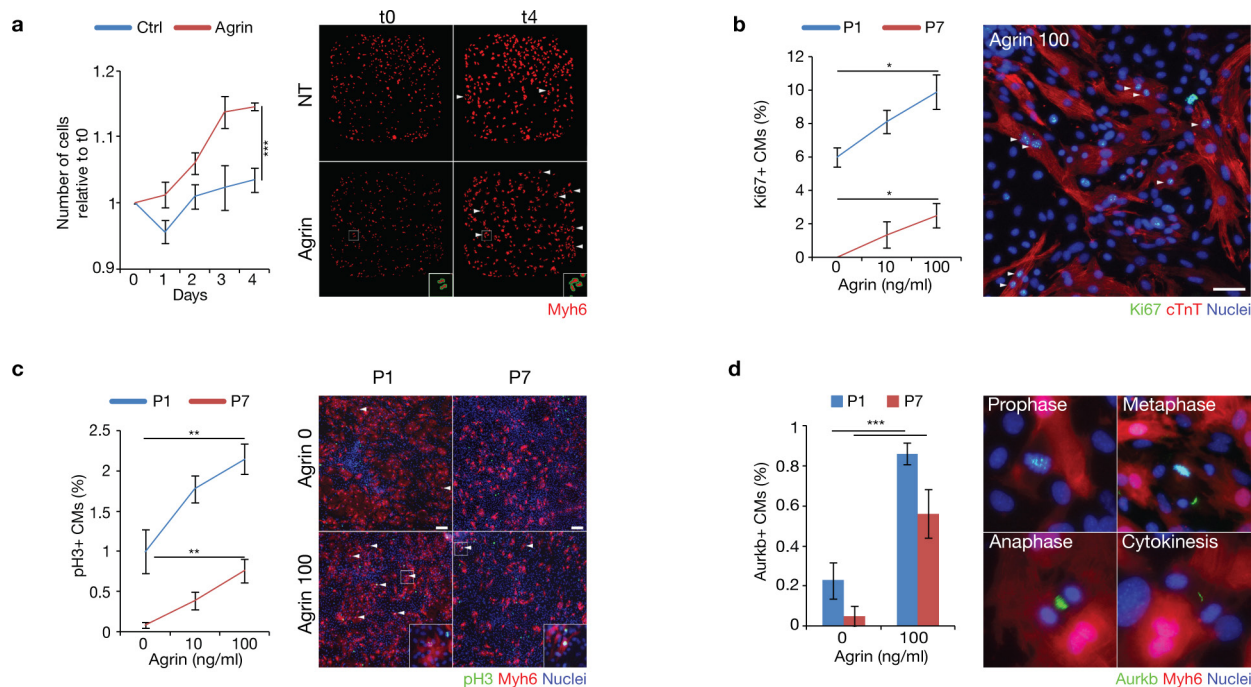


**Extended Data Figure 2 | Mass spectrometry results and validation.** **a**, Venn diagram representing the LC–MS results. **b**, qPCR analysis of genes obtained from the LC–MS in P1 and P7 whole-heart lysates.  $n=3$  P1 hearts and 3 P7 hearts.



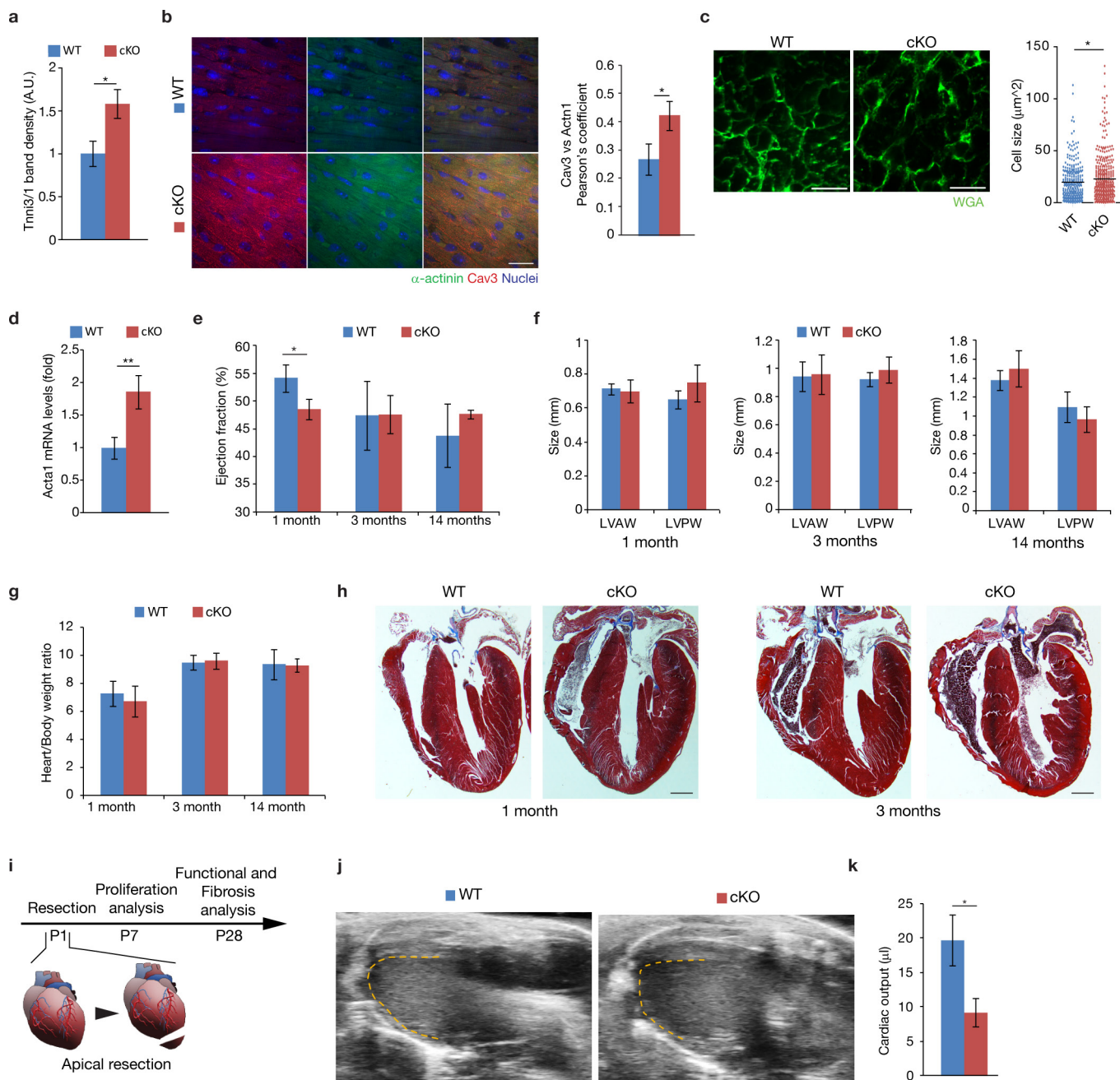
**Extended Data Figure 3 | P1 and P8 cardiac cell separation.** qPCR of mRNA from P1 and P8 heart lysates. qPCR analysis of six cell populations (fibroblasts, non-fibroblasts, cardiomyocytes, non-cardiomyocytes, endothelial cells, non-endothelial cells) for *CD90* (also known as *Thy1*, a fibroblast marker), *Myh6* (a cardiomyocyte marker) and *Pecam1* (Pecam, an endothelial cell marker) (for P1,  $n=4$  cardiomyocyte,

4 non-cardiomyocyte, 4 fibroblast, 7 endothelial cell, 7 non-endothelial cell samples and for P8  $n=2$  cardiomyocyte and 2 non-cardiomyocyte samples). Data are presented as mean  $\pm$  s.e.m. \* $P < 0.05$ , \*\* $P < 0.01$ , \*\*\* $P < 0.001$ ; statistical significance was calculated using a one-tailed *t*-test.



**Extended Data Figure 4 | Agrin induces cardiomyocyte proliferation *in vitro*.** **a-d**, Immunofluorescence evaluation of P1 and P7 cardiomyocytes ( $\text{cTnT}^+$  or  $\text{Myh6}^{\text{Cre/tdTomato}^+}$ , see Methods) cell number (**a**), cell-cycle activity (Ki67; **b**), mitosis (pH3; **c**) or cytokinesis (Aurkb, also known as Aim1; **d**) in response to agrin dosage *in vitro*. White arrowheads indicate proliferating cells. Analysis of five individual wells per treatment (**a**);  $n = 1,855$  P1 and  $1,328$  P7 cardiomyocytes pooled from the analysis of three P1 and four P7 samples (**b**);  $n = 11,450$  P1 and  $13,469$  P7

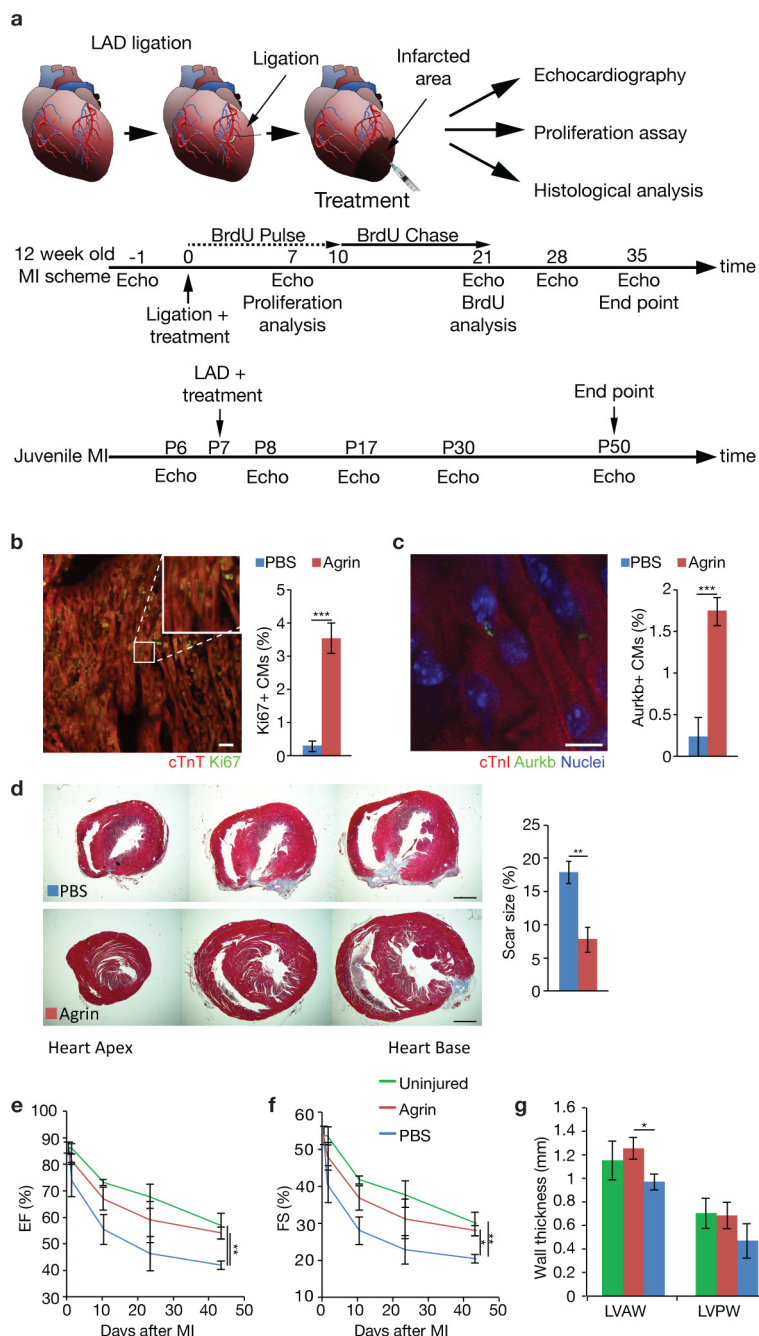
cardiomyocytes pooled from the analysis of four P1 and six P7 samples (**c**);  $n = 7,971$  P1 and  $3,856$  P7 cardiomyocytes pooled from the analysis of three P1 and three P7 samples (**d**). Scale bars,  $30\ \mu\text{m}$  (**b**) and  $100\ \mu\text{m}$  (**c**). Data are presented as mean  $\pm$  s.e.m. \* $P < 0.05$ , \*\* $P < 0.01$ , \*\*\* $P < 0.001$ ; statistical significance was calculated using an ANOVA followed by Dunnett's post hoc test relative to the control group (**a-c**) or using a one-tailed *t*-test (**d**).



#### Extended Data Figure 5 | Agrin-cKO cardiac characterization.

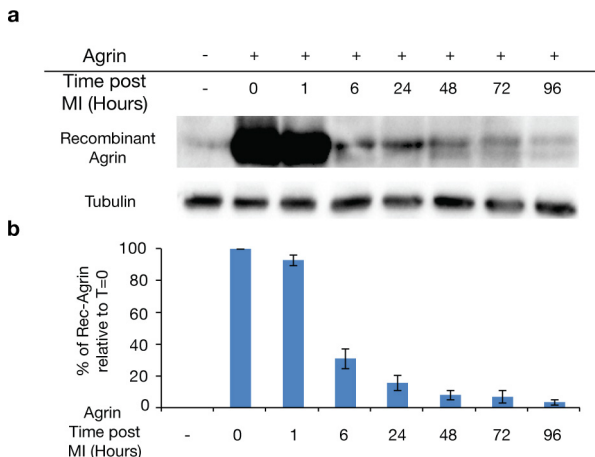
**a**, Tnni3:Tnni1 protein ratio in P8 agrin-cKO and wild-type mice.  $n=4$  wild-type and 7 cKO mice. **b**, Immunofluorescence analysis and Pearson's correlation coefficient analysis of P14 T-tubules by Cav3 colocalization with  $\alpha$ -actinin labelled z-lines.  $n=5$  wild-type and 6 cKO samples. **c**, Immunofluorescence analysis of WGA membrane staining in P1 wild-type and agrin-cKO depicting changes in cell size.  $n=2$  wild-type and 3 cKO samples. **d**, qPCR analysis of pathological hypertrophic marker *Acta1* in P1 wild-type and agrin-cKO heart lysates.  $n=21$  wild-type and 26 cKO samples. **e, f**, Serial echocardiographic measurements of ejection fraction (EF) and wall thickness of 1-, 3- and 14-month-old agrin cKO and wild-type mice.  $n=8$  mice per group at 1 month, 4 wild-type and 5 cKO

at 3 months and 4 wild-type and 3 cKO at 14 months. **g**, Heart to body weight ratio of 1-, 3- and 14-month-old agrin-cKO and wild-type mice.  $n=9$  wild-type and 4 cKO at 1 month, 4 wild-type and 5 cKO at 3 months and 6 wild-type and 5 cKO at 14 months. **h**, Histological sections of 1- and 3-month-old wild-type and agrin-cKO stained with Masson's trichrome. **i**, Scheme of P1 heart resection. **j**, Representative images of agrin-cKO and wild-type mice 28 days after resection at P1. **k**, Functional cardiac recovery measurement (cardiac output), 28 days after resection.  $n=5$  wild-type and 3 cKO mice (**j, k**). Scale bars, 20  $\mu$ m (**b**), 10  $\mu$ m (**c**) and 1 mm (**h**). Data are presented as mean  $\pm$  s.e.m. \* $P<0.05$ , \*\* $P<0.01$ ; Statistical significance was calculated using a one-tailed *t*-test.

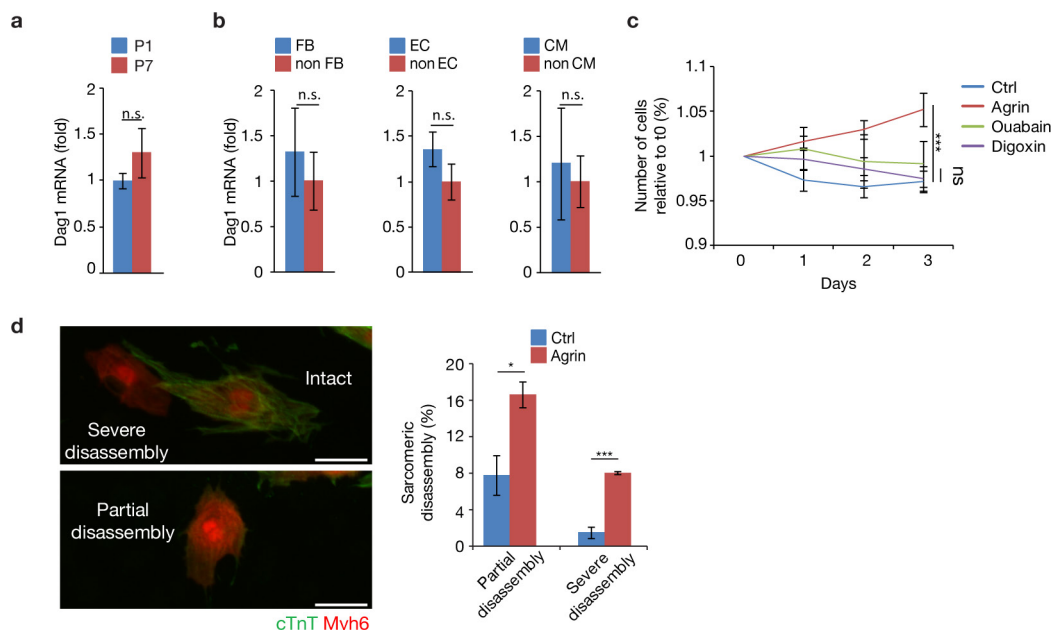


**Extended Data Figure 6 | Agrin induces cardiac regeneration in juvenile mice.** **a**, A schematic diagram depicting LAD ligation in juvenile and adult mice. **b, c**, *In vivo* evaluation of cardiomyocytes cell-cycle re-entry by Ki67 (**b**) or Aurkb (**c**) in heart sections seven days after myocardial infarction. *n* = 1,934 cardiomyocytes pooled from the analysis of three PBS-treated mice and three agrin-treated mice (**b**); *n* = 1,450 cardiomyocytes pooled from the analysis of three PBS- and six agrin-treated samples (**c**). **d**, Scar quantification based on Masson's trichrome staining of heart sections of PBS- and agrin-treated juvenile mice. Representative pictures are provided. *n* = 4 PBS- and 8 agrin-treated mice. **e–g**, Serial

echocardiographic measurements of ejection fraction (EF), fractional shortening (FS) and wall thickness of uninjured and injured PBS- and agrin-treated juvenile mice following myocardial infarction, according to the schema in **a**. *n* = 3 uninjured, 3 PBS- and 3 agrin-treated mice at day 13; and *n* = 4 uninjured, 5 PBS- and 9 agrin-treated mice at day 43. Scale bars, 10 μm (**b**), 20 μm (**c**) and 1 mm (**d**). Data are presented as mean ± s.e.m. \**P* < 0.05, \*\**P* < 0.01, \*\*\**P* < 0.001; statistical significance was calculated using a one-tailed *t*-test (**b–d**, **g**) or ANOVA followed by Dunnett's post hoc test relative to the control group (**e**, **f**).

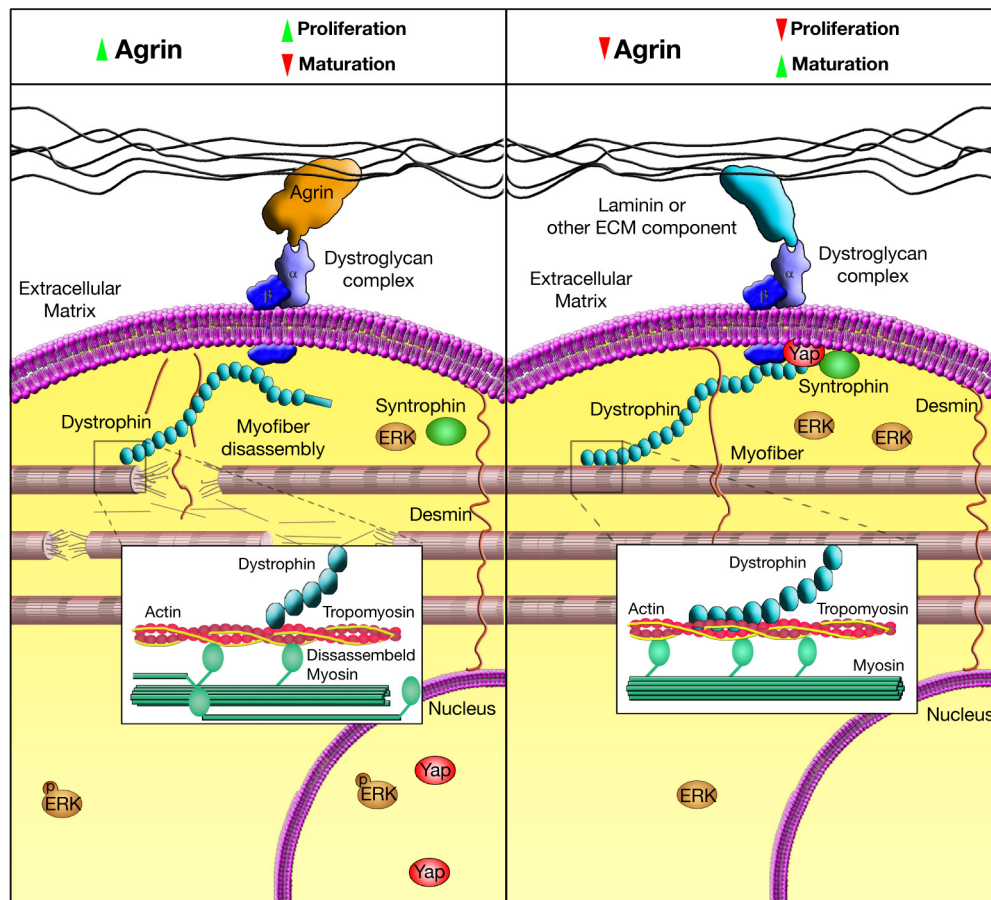


**Extended Data Figure 7 | Pharmacokinetics of agrin injection in injured adult hearts.** Mice were subjected to LAD ligation (as shown in Fig. 4a), and received either PBS or agrin treatment. Hearts were collected at respective time points after treatment, and were subjected to protein extraction and anti-His-tag immunoprecipitation using Ni-NTA resin. **a**, Representative western blot of agrin from relevant immunoprecipitation samples. Anti-tubulin western blot of respective total extracts, as immunoprecipitation loading control is shown at the bottom. **b**, The kinetics of recombinant agrin up to 96 h after treatment. The amount of agrin is presented as a percentage of the first time point ( $t = 0$ ), and normalized according to tubulin.  $n = 3$  repeats.



**Extended Data Figure 8 | Dag1 expression in P1 and P7 whole hearts and cardiac cell separation.** **a**, qPCR of *Dag1* mRNA from P1 and P7 heart lysates.  $n = 5$  P1 and 3 P7 samples. **b**, qPCR analysis of *Dag1* mRNA in distinct cardiac populations from P1 mice (fibroblasts, non-fibroblasts, cardiomyocytes, non-cardiomyocytes, endothelial cells, non-endothelial cells).  $n = 4$  cardiomyocyte, 4 non-cardiomyocyte, 4 fibroblast, 4 non-fibroblast and 7 endothelial and 7 non-endothelial cell samples. **c**, Serial immunofluorescence counting of Myh6-lineage-derived tdTomato-labelled cardiomyocytes treated with ouabain and digoxin which inhibit  $\text{Na}^+/\text{K}^+$  pumps. Quantification was made using acuman (see Methods).  $n = 31$

control, 16 agrin-, 11 ouabain- and 11 digoxin-treated individual wells per treatment. **d**, quantification of cardiomyocyte sarcomeric status by cTnT and Myh6-lineage immunofluorescence analysis of P7 agrin-treated cardiomyocytes cultured *in vitro* for three days.  $n = 2,222$  cardiomyocytes pooled from the analysis of three samples per group. Representative images of cardiomyocytes with intact, partially disassembled and severely disassembled sarcomeres are provided. Scale bars, 40  $\mu\text{m}$ . Data are presented as mean  $\pm$  s.e.m. \* $P < 0.05$ , \*\*\* $P < 0.001$ ; statistical significance was calculated using a one-tailed *t*-test (**a**, **b**, **d**) or ANOVA followed by Dunnett's post hoc test relative to control group (**c**).



**Extended Data Figure 9 | A model for the agrin–DGC–Yap signalling axis in cardiomyocyte maturation and cardiac regeneration.** Agrin triggers mild cardiomyocyte dedifferentiation and proliferation by modulation of DGC integrity and signalling. During neonatal stages agrin suppresses the maturation of the DGC. At P7, agrin levels are reduced

and ECM–DGC interaction through Dag1 promotes cardiomyocyte differentiation and maturation. Yap is tethered to the DGC upon cardiomyocyte maturation while upon agrin treatment, it translocates to the nucleus to facilitate cardiomyocyte cell-cycle re-entry.